J Nanostruct 9(2): 202-210, Spring 2019

RESEARCH PAPER

Structural, Electrical, and Impedance Spectroscopy Studies of Barium Substituted Nano Calcium Ferrites Synthesized by Solution Combustion Method

Puttaraju Shankar[1,2,*], Bhavyashri Shetty[3], Antony Lazor Jayasheelan[4], Nanja Reddy Sivasankara Reddy[5], Challa Seshu Prakash[6]

[1] *Department of Physics, Sai Vidya Institute of Technology, Bengaluru, India*

[2] *Visveswaraya Technological University, Belagavi, India*

[3] *Department of Physics, Don Bosco Institute of Technology, Bangalore, India*

[4] *Department of Physics, Maharani's Science College for Women Bengaluru, India*

[5] *Department of Physics, Presidency University , Bangalore, India*

[6] *Department of Physics, SJC Institute of Technology, Chikkaballapura, India*

ARTICLE INFO

Article History:
Received 14 December 2018
Accepted 06 March 2019
Published 01 April 2019

Keywords:
Barium Calcium Ferrite
Complex Impedance Spectroscopy Dielectric Properties
Electric Modulus
Nano-Ferrites

ABSTRACT

Barium substituted nano crystalline ferrites with chemical composition $Ba_xCa_{1-x}Fe_2O_4$ (x =0.0 to 0.25) BCAF were prepared by novel solution combustion method. The phase formation of mixed spinal structured ferrites was confirmed by PXRD analysis. The average crystallite size was calculated using Debye-Scherrer formula and it was found to be in the range of 27-44 nm. Surface morphology was analyzed by SEM, it reveals the highly porous nature of the synthesized samples. Nano crystalline nature of synthesized samples was confirmed by TEM and particle size of the samples was further studied using TEM.The dielectric constant, dielectric loss factor (tan δ) and AC conductivity (σ_{ac}) of the samples were measured using LCR meter in the frequency range of 100 Hz–5 MHz at room temperature. The dielectric constant of the synthesized ferrite samples was found to decrease with increase in frequency and finally reaches a constant value at higher frequencies which is typical behavior of dielectric ferrites. The observed dielectric dispersion is of Maxwell-Wagner type interfacial polarization. The contribution of grain boundary resistance has been studied from the cole-cole plots. The impedance spectroscopy analysis confirms the non-Debye type of conductivity relaxation for the nanocomposite. The high value of the dielectric constant makes the material suitable for miniature memory devices based capacitive components or energy storage devices. The samples also show low dielectric losses at high frequency region which makes them suitable for high frequency applications and also long relaxation time of BCAF nano composites could makes them suitable for nano scale spintronic devices.

How to cite this article
Shankar P, Bhavyashri S, Jayasheelan AL, Sivasankara Reddy NR, Prakash CS. Structural, Electrical, and Impedance Spectroscopy Studies of Barium Substituted Nano Calcium Ferrites Synthesized by Solution Combustion Method. J Nanostruct, 2019; 9(2): 202-210. DOI: 10.22052/JNS.2019.02.002

INTRODUCTION

Ferrites having the general formula of MFe_2O_4 (M= Ca^{2+}, Co^{2+}, Ni^{2+}, Mn^{2+}, Mg^{2+}, Zn^{2+} etc) are the group of hybrid functional materials. They are very superior over other nano materials as they can exhibit very good electrical and magnetic properties simultaneously at high frequency regimes. These materials are very useful in designing electrical, magnetic, microwave and other advanced electronic devices [1]. They also find wide range of technological applications in information storage systems, transformer core, multilayered chip inductors, magneto caloric refrigeration and magnetic diagnostics [1-3] due to their predominant properties such as high electrical resistivity, high saturation magnetization, low power losses and

* *Corresponding Author Email: shankarp401@gmail.com*

high initial permeability [4,5]. The main advantage of these ferrites is due to their large compositional variability, which can be achieved by the substitution of different cations in the host crystal structure (at tetrahedral and octahedral sub-lattices) and as a result various physical, electrical, structural and magnetic properties can be tuned, which makes them excellent multi functional materials [6]. Also due to the combined effect of magnetic and electrical properties ferrites they are very good candidate for multiferroic materials. Recently kumar et al have reported that ferrites behave like multiferoic materials [7].

The structural and electrical properties can be improved by the proper choice of divalent cations to replace Ca^{2+} ions, in the parent lattice of calcium ferrite which causes a structural variation in the host lattice. The distribution of cations among A-sites and B-sites is responsible for mobility of the charge carriers which plays a very important role in the observed electrical and dielectric behaviors (dielectric constant and losses) in ferrites [8, 9]. Calcium ferrite is a mixed spinal ferrite along with moderate magnetization, magneto resistance and very high magneto crystalline anisotropy. The preparation methods, substitutions and the sintering temperature have profound influence on the structural, electrical and magnetic properties of ferrites [10, 11]. Several methods have been employed to synthesize the nano ferrites with controlled microstructure and particle size including co-precipitation [12], sol–gel [13], reverse micelles [14], hydrothermal [15] and solvothermal [16]. The Impedance spectroscopy is an important tool to study the electrical conduction behavior of the ferrites. The complex impedance studies were carried out as a function of frequency of the applied AC field to understand the dielectric dispersion and relaxation behavior of synthesized nano ferrites.

The reports found on the literature on dielectric feature and impedance spectroscopy of Barium substituted Calcium ferrite is scarce. This material has been extensively studied due to its high resistivity. So the analysis in order to understand the source of resistance, contribution of resistances from grain boundaries and grains, to resolve the relaxation contributions and conduction phenomenon in these materials is more intriguing. As per the best of our knowledge, many researchers have tried to investigate and analyze the properties like structural, electrical and dielectrical properties of ferrites using different experimental techniques but an adequate analysis of impedance spectroscopy and electric modulus of Ba substituted calcium ferrite is still lacking and offers further investigations.

In the present work we attempt to study the influence of Ca: Ba ratio on the structural, electrical and dielectric properties of the barium doped calcium ferrites synthesized by novel solution combustion method. The solution combustion method offers many advantages like it is rather simple, economical, less time consuming and scalable for industrial applications compare to other methods. The variations in the conductivity, dielectric constant and dielectric loss tangent, complex impedance, electric modulus with composition, frequency have been studied and the results are discussed.

MATERIALS AND METHODS

The barium substituted calcium ferrites $Ba_xCa_{1-x}Fe_2O_4$ (where x= 0.00 to 0.25 in steps of 0.05) **BCAF** were prepared by solution combustion method [17] using stoichiometric ratio of oxidizer and fuel. AR grade (Aldrich) Barium nitrate ($Ba(NO)_3.6H_2O$), ferric nitrate ($Fe(NO_3)_3$) and Calcium nitrate hexa hydrate ($Ca(NO_3)_2.6H_2O$ are used as oxidizers and ODH used as a fuel [18]. The metal nitrates and ODH were dissolved in double distilled water using a magnetic stirrer to obtain the uniform mixture. This mixture was taken in a Pyrex dish and kept in a pre-heated muffle furnace maintained at 450 ± 10°C. Initially, the solution boils and subsequently frothed to yield fine brown coloured powder. The combustion process completes in 20 min. The obtained samples were then ground properly to get fine powder. The structural studies were carried out using X-ray diffractometer and the average size was calculated using Debye-Scherrer formula, $S = k\lambda / \beta\cos\theta$ where k = 0.9 is the correction factor to account for the particle shapes, β is the full width at half maximum (FWHM) of the most intense diffraction peak, λ is the wavelength of a Cu-K_α radiation = 1.5406 Å and θ is the Bragg's angle. The surface morphology of all the samples was studied by SEM (JSM-6490) at a voltage of 5 kV. The average particle size is estimated by TEM micrographs using Image J software were taken by FETEM with electron energy of 200 kV. The dielectric and a. c. conductivity studies were carried out using programmable impedance analyzer (Waynkerr 6500 B) at room temperature in the frequency range of 100Hz-5MHz.

RESULTS AND DISCUSSIONS

Structural properties

The Powder X-ray diffraction patterns of all samples of BCAF are shown in the Fig. 1. PXRD pattern reveals that the synthesized samples were found to be polycrystalline in nature having orthorhombic structure and it is well matched with JCPDS No 32-168. All the diffraction peaks were indexed as (320), (2 01), (131), (311), (141) (401) and (161) which confirms the phase formation of the prepared ferrites with space group Pnam (no. 62). Broad diffraction peaks indicates that the ferrite particles are of nano-sized. The crystallite size of samples were estimated using Debye-Scherrer formula and it is found that, the average crystallite size increases with increase in concentration of Ba^{2+}.

The increase in crystallite size is due to the substitution of elements at different site that changes the unit cell parameters or volume because of the difference in ionic radii. In the present system, radius of Ba^{2+} (=1.35 Å) is larger than that of Ca^{2+} (1.00Å), Therefore, substitution of Ba^{2+} at the A-site may results in an increase in the crystal size as its composition is varied. The variation of crystallite size with different concentration of the Ba is shown in the Table 1.

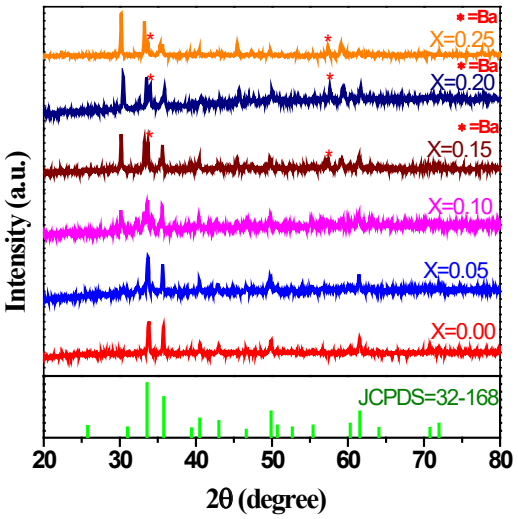

Fig. 1. XRD patterns for $Ba_xCa_{1-x}Fe_2O_4$ (x=0.05, 0.1, 0.15, 0.2, 0.25).

Morphology analysis by SEM

The scanning electron micrographs (SEM) of the calcium nano ferrite sample x=0.00 are shown in Fig. 2a and Fig. 2b, the barium substituted calcium nano ferrite sample for the concentrations x=0.25 are shown in Fig. 2c and Fig. 2d. The SEM micrographs shows the presence of uniform mono phase microstructure. The micrographs reveal that the synthesized ferrites are highly porous in nature, which is due to the evolution of the gases during the solution combustion process. The porous structure has a large specific area which results in the improvement of active surface suitable for many useful applications in sensor based devices [19]. SEM micrographs also show that sub micrometer sized primary particles are agglomerated into the larger secondary particles with slightly spherical shapes and making a compact network, hence these materials may be used for frequency dependent conductivity applications like EMI shielding, antenna and core of inductors etc [20]. The agglomerated nature is usually observed in many nano crystalline ferrites. The EDAX measurements for calcium nano ferrite for x=0.00 is shown in Fig. 3a and for the concentrations x=0.25 are shown in Fig. 3b. It reveals that the Ca: Ba: Fe ratio in the matrix is close to the nominal compositions with an overall a slight excess of Fe observed. The EDAX results suggest that the precursors have undergone the chemical reaction fully to form the BCAF ferrite materials.

Particle size analysis by TEM

The TEM micrographs of $CaFe_2O_4$ are shown in Fig. 4. The images show slightly spherical particles,

Table 1. Crystallite size D, Sherrer method, Real part of dielectric constant (ε'), Imaginary part of dielectric constant (ε''), tangent loss(Tanδ),AC conductivity, Relaxation frequency(fr), Relaxation time(τr) for $Ba_xCa_{1-x}Fe_2O_4$ (x=0.05, 0.1, 0.15, 0.2, 0.25).

Parametrs/compsition	X=0.0	X=0.05	X=0.1	X=0.15	X=0.2	X=0.25
Average crystallite size D_p(nm)	40.43	40.92	41.31	42.92	48.52	50.88
ε'(1 KHz)	642	135.16	30.21	38.74	20.68	18.64
Tanδ (1 KHz)	2.002	0.812	0.396	0.527	0.376	0.462
σ_{AC} (1 KHz)	1.78×10^{-5}	3.84×10^{-6}	9.42×10^{-6}	2.83×10^{-6}	3.17×10^{-6}	3.71×10^{-6}
ε'(1 MHz)	17.97	23.07	13.25	14.57	11.57	9.46
Tanδ (1 MHz)	0.164	0.129	0.462	0.045	0.039	0.527
σ_{AC} (1 MHz)	6×10^{-3}	9×10^{-3}	9.9×10^{-3}	2.1×10^{-3}	16.5×10^{-3}	17.6×10^{-3}
f_r(Hz)	100×10^{3}	45×10^{3}	5×10^{2}	4×10^{3}	0.8×10^{3}	0.8×10^{3}
τ_r(s)	1×10^{-5}	2.2×10^{-5}	2×10^{-3}	2.5×10^{-4}	1.25×10^{-3}	1.25×10^{-3}

with less regularity in size. The particles are agglomerated due to their slow growth during the solution combustion process [21]. The particles size were measured using "ImageJ" software. The particle size obtained from TEM was about 30 nm and the results are in very good agreement with the average crystallite size calculated by Debye-Scherer formula using XRD data. The HRTEM image has a lattice spacing of 3.5 nm which confirms the crystalline nature of the sample.

Electrical properties

The study of electrical properties of ferrites is very useful, in order to unfold their suitability for the devices of frequency dependant applications. These properties depend upon materials composition, method of preparation, sintering temperature and cation positions in the unit cell. Dielectric parameters like dielectric constant, complex dielectric constant, dielectric loss and ac conductivity of $Ba_xCa_{1-x}Fe_2O_4$ (where x= 0.00 to 0.25 in steps of 0.05) ferrites were investigated in the frequency range 100Hz–5MHz at room temperature.

A.C. conductivity

The conduction mechanism in ferrite sample is mainly due to charge libration and hopping of electrons between the ions of same element which are formed during sintering, which exist in more than one valence state (Fe^{2+} and Fe^{3+})

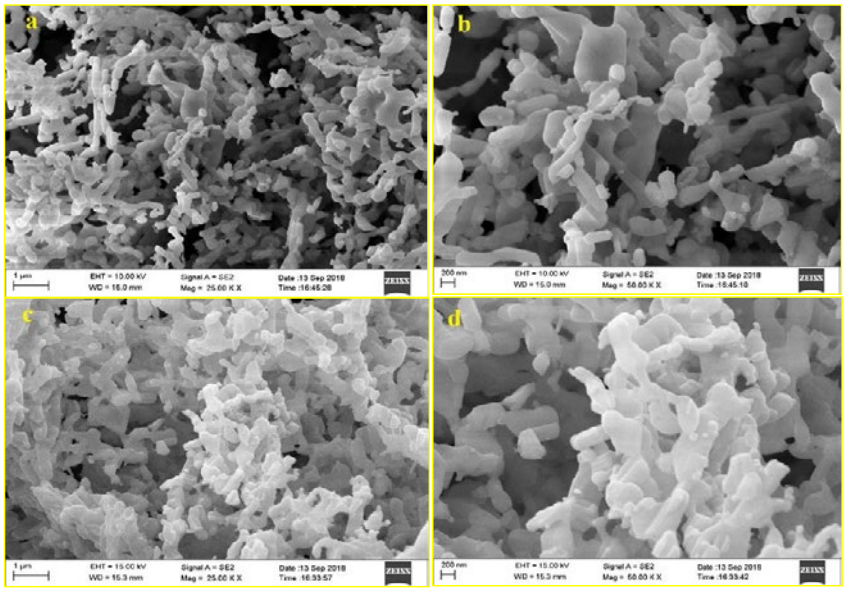

Fig. 2. a,b) Scanning electron microscopy of $Ba_xCa_{1-x}Fe_2O_4$ for x=0.00 c,d)Scanning electron microscopy of $Ba_xCa_{1-x}Fe_2O_4$ for x=0.25.

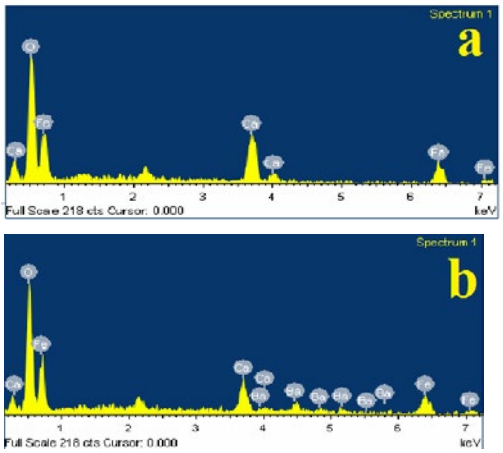

Element	Weight%	Atomic%
O K	26. 61	53.66
Ca K	17. 35	13.97
Fe K	56. 04	32.37
Totals	100.00	

Element	Weight%	Atomic%
O	22.30	51.69
Ca	10.47	9.69
Fe	51.96	34.50
Ba	15.27	4.12
Total	100.00	

Fig. 3. a) FESEM Edax of $Ba_xCa_{1-x}Fe_2O_4$ for x=0.0 b) FESEM Edax of $Ba_xCa_{1-x}Fe_2O_4$ for x=0.25.

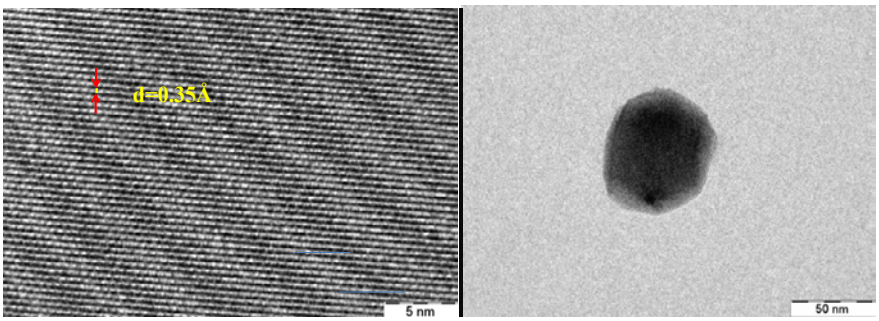

Fig.4. TEM Image of $CaFe_2O_4$ Parent sample.

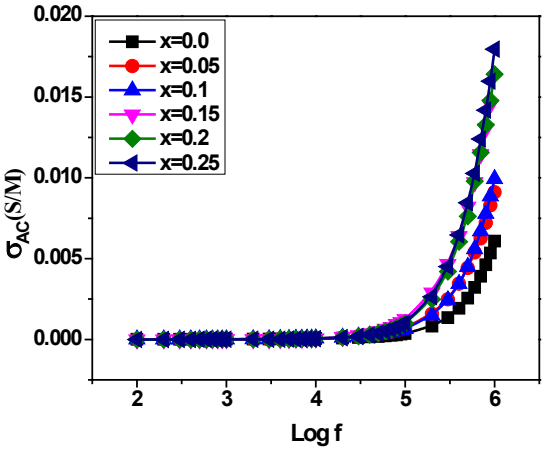

Fig. 5 A.C Electrical conductivity (σ_{ac}) v/s Log f of $Ba_xCa_{1-x}Fe_2O_4$ (x=0.05, 0.1, 0.15, 0.2, 0.25)

and distributed randomly at B-site as explained by verwey et.al [22]. The electronic exchange between Fe^{2+} and Fe^{3+} ions results in the local displacement of charges in the direction of the applied field, which is responsible for polarization in ferrites [23]. The rate of hopping depends on the concentration of Fe^{2+} and Fe^{3+} ion pairs at B-site. Since the increase in frequency enhances electron hopping frequency of the charge carriers between Fe^{2+} and Fe^{3+} the conductivity increases. The dependence of conductivity on frequency can also be explained on the basis of poloron hopping model reported by austin-mott [24] according to which σ_{AC} shows increasing trend with increase in frequency for small range poloron hopping

The equation for total electrical conductivity is given by

$$\sigma(f,T)= \sigma_{dc}(T) + \sigma_{ac}(f,T) \quad (1)$$

σ_{dc} is the d.c conductivity depends only on temp, the second term σ_{ac} is the A.C conductivity which depends both on temperature and frequency attributed to the electron hopping mechanism at the B-site. The frequency depandance of σ_{ac} is expressed by the formula

$$\sigma_{ac}(f)=Af^n \quad (2)$$

where A and n are constants.

The variation of σ_{ac} with frequency is shown in the Fig. 5.It is also observed from the figure that the value of σ_{ac} shows almost frequency independent nature up to frequency of 60 kHz, as per the frequency independent conductivity observed in the case of band conduction. Whereas beyond this frequency 60 kHz (hopping frequency) the value of σ_{ac} increases with frequency for all the samples of BCAF. The transition frequency from σ_{dc} to σ_{ac} is termed as hopping frequency, indicating the transition from band conduction to poloron hopping conduction [25,26].

Also it can be seen from the figure that the conductivity increases with increase in concentration of Ba^{2+} at the expense of Ca^{2+}. This increase in conductivity is due to increase in electron hopping process which arises due to the reduction in the field strength of surrounding ionic sites (Ca^{2+}=0.35 and Ba^{2+}=0.27[27]) at Fe ions site.

Dielectric constant

The frequency dependent complex dielectric function is generally described using the expression:

$$\varepsilon^*(\omega)=\varepsilon'(\omega) - i\varepsilon''(\omega) \quad (3)$$

ε′ is the real part of the dielectric constant, ε′′ is the imaginary part of the dielectric constant.

$$\varepsilon' = C\, d / (\varepsilon_o A) \quad (4)$$

Where C, d, A and ε_o represent the capacitance (in farad), thickness (in meters), cross-sectional

area of the flat surface and constant of permittivity for free space ($\varepsilon_o = 8.86 \times 10^{-12}$ F/m).

Fig. 6 describes the variation of (ε'). The decrease in real part of dielectric constant (ε') with increase in frequency is explained on the basis of relative frequencies of the applied electric field and electron hopping. If the frequency of the electron hopping between the Fe^{3+} and Fe^{2+} ions at octahedral site (B-site) is higher when compared to the frequency of the applied AC field, the hopping of electrons can able to interact with the field reversals of the applied electric field very easily, resulting in a higher value of dielectric constant (ε'). This tendency holds good for low frequencies. Whereas, at higher frequencies since the hopping electrons are required to move across a resistive body of the sample, they can no longer follow the field reversals of frequency of the applied field, which results in phase lagging and lowering of the dielectric constant (ε'). Consequently, the electron exchange between Fe^{3+} and Fe^{2+} is perturbed at high frequencies, which explains the lower value of dielectric constant (ε') at high frequencies, which is in good agreement with the Koops' model [28]. According to Koop's model, the ferrite consists of two layers of Maxwell-Wagner type [29], known as the grains (a more conducting layer) and the grain boundaries (a poor conducting layer). The number of grain boundaries increases with decrease in grain size, which contributes to the dielectric constant at lower frequencies while the grains have low dielectric constants and are effective at high frequencies. Further the species contributing to the polarizability lags behind the applied field.

From the figure it is also observed that dielectric constant is maximum for the sample for the composition x=0.00 compared to the other samples, this increased dielectric dispersion can be explained on the basis of concentration of ferrous ions at the octahedral site. For x=0.00 the concentration of ferrous ions is higher compared to the other compositions of BCAF ferrites at the octahedral site. Due to this fact it is possible for these ions to get polarized maximum. Whereas for the other compositions the Ba ions increases at the octahedral site causing the decrease in the number of ferrous ions responsible for polarization [30], resulting in the low value of dielectric constant.

Dielectric loss(Tan δ)

The dielectric loss factor tanδ estimates the loss of energy within the material which occurs due to the phase difference at a particular frequency and is given by the relation:

$$\mathrm{Tan}\delta = \frac{\varepsilon''}{\varepsilon'}$$

Fig. 7 shows the variation of dielectric loss with the frequency. The value of Tan δ depend upon no of factors such as stoichiometry, Fe^{2+} content and structural homogeneity which in turn depend upon the composition and sintering temperature of the samples[31]. It can be seen from the figure that the value of tanδ for all the samples of BCAF has been found to decrease with increase in frequency. This nature of dielectric loss can be explained on the basis of koops phenomenological theory of dielectrics [28]. As per this theory at lower frequencies the value of resistivity is high due to grain boundaries hence more energy is required exchange of electron between Fe^{2+} and Fe^{3+} ions resulting in high energy loss leading to

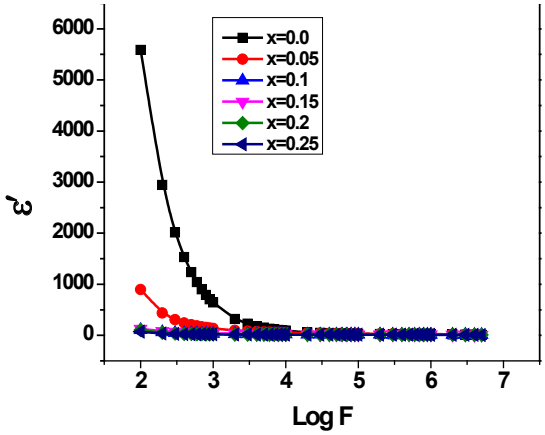

Fig. 6. (ε') v/s Log f $Ba_xCa_{1-x}Fe_2O_4$ (x=0.05, 0.1, 0.15, 0.2, 0.25)

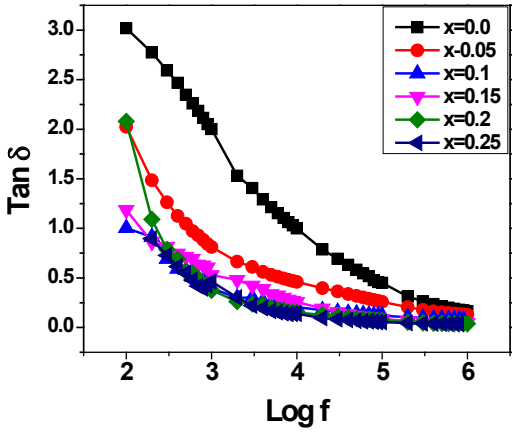

Fig. 7. Tanδ v/s Log f $Ba_xCa_{1-x}Fe_2O_4$ (x=0.05, 0.1, 0.15, 0.2, 0.25)

large value of tanδ. Where as at high frequencies small energy is enough for the electron transfer due to low resistance resulting in low energy loss. Many partial peaks can be observed from the figure for all the compositions of BCAF, the peaks are formed whenever the frequency of the hopping charge carriers coincides with the frequency of the applied field. This behavior of ε′ and tan δ observed for BCAF ferrite samples are in good agreement with those reported by S.M. Ramay et al, M. Hashim *et al* and T. Ramesh et al [32-34]

Impedance analysis

Fig. 8 shows the complex impedance spectra for all the compositions of BCAF at room temperature. Impedance spectroscopy is an important method to understand the electrical properties of ferrites. According to Maxwell-wagner model a ferrite material is assumed as piled up layers of conducting plates (grains) separated by resistive plates (grain boundaries). The impedance response of such materials may consists of contributions from the grains, grain bounderies and the material electrodes in the order of decreasing frequency. The impedance of grains, grain boundaries and impedance electrodes results in a separate semicircles in complex impedance plane as they posses different relaxation times.

According to the cole-cole type of distribution, complex impedance is composed of two overlapping semicircles.

First one at low frequency corresponds to grain boundary and the second one at high frequency is due to the grain, based on the distribution of relaxation times [35]. If the time constant of the different process differs by a factor of less than hundered then impedance responses due to grain boundary and the grain may overlap.

It can be noticed from the figure that the complex impedance spectra for all the compositions of BCAF shows only one semi circular arc corresponding to the grain boundary, which indicates that grain boundary resistance is very high for all the samples. The high value of the grain boundary resistance may be due to the increased disorder atomic arrangement, increased surface to volume ratio, porosity and decrease of Fe^{3+} ions. Among the different compositions of BCAF, the grain boundary resistance is small for x= 0.00 comparatively. Further from the impedance plots the data do not represent the full semi circle rather they are partial semicircles. Also it is observed that the centre of semicircles lies below the abscissa (Z′) axis which suggests the dielectric relaxation is of non-Debye type in the all BCAF samples. It is also noticed that the radius of the semicircle is different for different samples because of variation in the relaxation time [36,37].

Electric Modulus analysis

From the analysis of complex electric modulus the electrical responses of the material and electrical relaxation of ionic solids can be understood. Typical features M* as a function of frequency may be broad, asymmetric peak in the imaginary part and a sigmoidal step in the real part. In order to reconfirm the relaxation behavior in BCAF sample the real and imaginary parts of the electric modulus are calculated using the relations

$$M^*=\frac{1}{\varepsilon^*},\quad M'=\frac{\varepsilon'}{(\varepsilon')^2+(\varepsilon'')^2},\quad M''=\frac{\varepsilon''}{(\varepsilon')^2+(\varepsilon'')^2} \qquad (6)$$

Frequency dependence of the M′ for the BCAF samples are illustrated in the Fig. 9. The M′ shows continuous dispersion with increase in frequency.

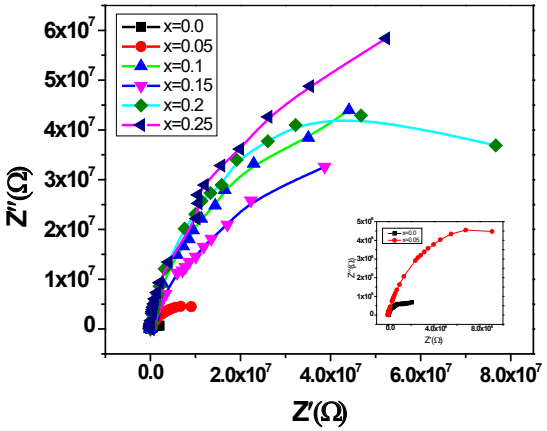

Fig. 8. Cole-Cole plots for $Ba_xCa_{1-x}Fe_2O_4$ (x=0.05, 0.1, 0.15, 0.2, 0.25)

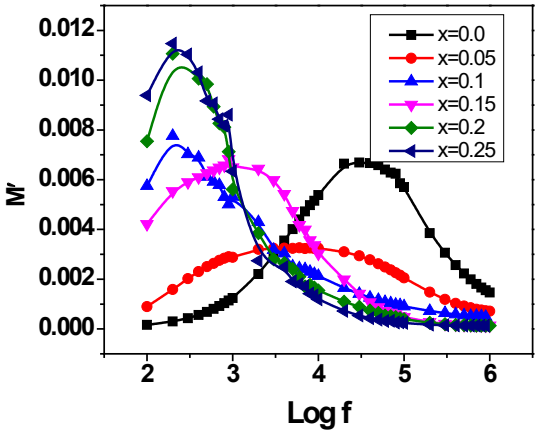

Fig. 9. (M′) v/s Log f of $Ba_xCa_{1-x}Fe_2O_4$ (x=0.05, 0.1, 0.15, 0.2, 0.25)

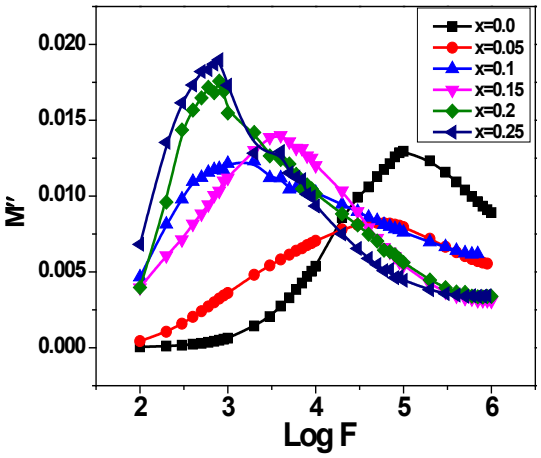

Fig. 10. (M'') v/s Log f of $Ba_xCa_{1-x}Fe_2O_4$ (x=0.05, 0.1, 0.15, 0.2, 0.25)

Dispersion at low frequency suggest that the conduction phenomenon due to short range mobility of charge carriers. It is also found the dispersion shifts towards the high frequency region for the Barium content X=0.15, which suggests the long range mobility of the charge carriers [38].

The variation of M'' as a function of frequency of different Ba concentration is illustrated in Fig. 10. The Fig shows the well resolved peak in the pattern. The peak in the low frequency region determines the range in which the charge carriers can move over long distances. The peak towards the high frequency region determines the range in which the charge carrirs are spatially confined to their potential wells and being mobile over short distances [39].

Thus the peak frequency indicates the transition from long range to short range mobility with increase in frequency. The peak frequency shifts towards the left for the higher values composition. The characteristic frequency at which M'' is maximum correspond to relaxation frequency form which relaxation time can be evaluated using the formula. $\tau_{M''} = [1/(2\pi f_{M''})]$. The relaxation time and frequency are provided in Table 1. The given plot is asymmetric nature with respect to peak maxima and the peaks are considerably broader on either side of the maxima, this type of nature is being the consequence of the distributions relaxation time due to non-debye nature of the material. It is observed that τ is of the order milliseconds , it is noteworthy that τ is typically of the order of 100 ns in semiconductors [39] and they are on the order of picoseconds in bulk materials due to the high density of scattering centers [40,41]. Such a long dielectric spin –relaxation time in the BCAF nano composites can be very useful in nano scale spintronic devices.

CONCLUSION

The present work summarizes the sol–gel synthesis of Ba^{2+} doped $Ba_xCa_{1-x}Fe_2O_4$ (where x=0.0, 0.05, 0.1, 0.15.0.2& 0.25) by solution combustion method using ODH as a fuel. The PXRD patterns confirm the formation of single phase. The crystallite size was estimated through the Scherer's formula is found to be in the range 27-44 nm. AC conductivity increases linearly with the applied field. The real and imaginary part of permittivity have been found to decreases with increase in frequency of the applied field as well as with the dopant concentration due to electronic hopping between Fe^{3+} and Fe^{2+}. Complex impedance analysis for the ferrites under study reveals that grain boundary resistance is dominant for all the Ba-substituted calcium ferrite. Also, the impedance and modulus analysis confirms the presence of non-Debye type of relaxation in Ba substituted Calcium ferrite. The synthesized material possesses lower value of dielectric loss at high frequency which are suitable frequency dependant automotive applications and long dielectric spin times have also been determined from the electric modulus spectra that make the BCAF nano composite as a promising candidate for nano scale spintronic devices.

AKNOWLEDGEMENT

The authors would thank Principal and management of Sai Vidya institute of technology Bangalore and A.C.S College of Engineering, Bangalore. We are thankful Dr. B.M. Nagbhushan. H.O.D, Department of chemistry, MSRIT, Bangalore, we are also thankful to Dr. Murugendrappa, Department of Physics, BMSCE for providing the lab facilities to carry out electrical properties.

CONFLICT OF INTEREST

The authors declare that there are no conflicts of interest regarding the publication of this manuscript.

REFERENCES

1. Praveena K, Sadhana K, Bharadwaj S, Murthy SR. Development of nanocrystalline Mn–Zn ferrites for high frequency transformer applications. Journal of Magnetism and Magnetic Materials. 2009;321(16):2433-7.
2. Abasht B, Beitollahi A, Mirkazemi SM. Processing, structure and magnetic properties correlation in co-precipitated Ca-ferrite. Journal of Magnetism and Magnetic Materials. 2016;420:263-8.
3. Jagadeesha Angadi V, Anupama AV, Kumar R, Matteppanavar S, Rudraswamy B, Sahoo B. Observation of enhanced magnetic pinning in Sm 3+ substituted nanocrystalline Mn Zn ferrites prepared by propellant chemistry route. Journal of Alloys and Compounds. 2016;682:263-74.
4. Praveena K, Sadhana K, Bharadwaj S, Murthy SR. Fabrication of

dc–dc converter using nanocrystalline Mn–Zn ferrites. Materials Research Innovations. 2010;14(1):102-6.
5. Thakur S, Katyal SC, Gupta A, Reddy VR, Sharma SK, Knobel M, et al. Nickel–Zinc Ferrite from Reverse Micelle Process: Structural and Magnetic Properties, Mössbauer Spectroscopy Characterization. The Journal of Physical Chemistry C. 2009;113(49):20785-94.
6. G. Bate,in: D. J. Craik(Ed.), MagneticOxides, Part2 Wiley Inter-Science, New York,1975p.703.
7. Kumar S, Alimuddin, Kumar R, Dogra A, Reddy VR, Banerjee A. Mössbauer and magnetic studies of multiferroic Mg0.95Mn0.05Fe2−2xTi2xO4 system. Journal of Applied Physics. 2006;99(8):08M910.
8. Chandramohan P, Srinivasan MP, Velmurugan S, Narasimhan SV. Cation distribution and particle size effect on Raman spectrum of CoFe2O4. Journal of Solid State Chemistry. 2011;184(1):89-96.
9. A. Goldman, Modern Ferrite Technology, Marcel Dekker, Inc., NewYork,1993.
10. Jacob BP, Kumar A, Pant RP, Singh S, Mohammed EM. Influence of preparation method on structural and magnetic properties of nickel ferrite nanoparticles. Bulletin of Materials Science. 2011;34(7):1345-50.
11. Uday Bhasker S, Vijaya Kumar Y, Ramana Reddy MV. Preparation and Characterization of Cobalt Magnesium Nano Ferrites Using Auto-Combustion Method. Advanced Materials Research. 2012;584:280-4.
12. Ali I, Islam MU, Ishaque M, Khan HM, Naeem Ashiq M, Rana MU. Structural and magnetic properties of holmium substituted cobalt ferrites synthesized by chemical co-precipitation method. Journal of Magnetism and Magnetic Materials. 2012;324(22):3773-7.
13. Chen D-H, He X-R. Synthesis of nickel ferrite nanoparticles by sol-gel method. Materials Research Bulletin. 2001;36(7-8):1369-77.
14. Gubbala S, Nathani H, Koizol K, Misra RDK. Magnetic properties of nanocrystalline Ni–Zn, Zn–Mn, and Ni–Mn ferrites synthesized by reverse micelle technique. Physica B: Condensed Matter. 2004;348(1-4):317-28.
15. Peng J, Hojamberdiev M, Xu Y, Cao B, Wang J, Wu H. Hydrothermal synthesis and magnetic properties of gadolinium-doped CoFe2O4 nanoparticles. Journal of Magnetism and Magnetic Materials. 2011;323(1):133-7.
16. Wang J, Ren F, Yi R, Yan A, Qiu G, Liu X. Solvothermal synthesis and magnetic properties of size-controlled nickel ferrite nanoparticles. Journal of Alloys and Compounds. 2009;479(1-2):791-6.
17. Raveendra RS, Prashanth PA, Hari Krishna R, Bhagya NP, Nagabhushana BM, Raja Naika H, et al. Synthesis, structural characterization of nano ZnTiO3 ceramic: An effective azo dye adsorbent and antibacterial agent. Journal of Asian Ceramic Societies. 2014;2(4):357-65.
18. Patil KC, Hegde MS, Rattan T, Aruna ST. Chemistry of Nanocrystalline Oxide Materials: WORLD SCIENTIFIC; 2008 2008/09.
19. Hemeda OM, Mostafa NY, Abd Elkader OH, Hemeda DM, Tawfik A, Mostafa M. Electrical and morphological properties of magnetocaloric nano ZnNi ferrite. Journal of Magnetism and Magnetic Materials. 2015;394:96-104.
20. Yang C, Liu F, Ren T, Liu L, Feng H, Wang AZ, et al. Fully integrated ferrite-based inductors for RF ICs. Sensors and Actuators A: Physical. 2006;130-131:365-70.
21. Mali A, Ataie A. Influence of Fe/Ba molar ratio on the characteristics of Ba-hexaferrite particles prepared by sol–gel combustion method. Journal of Alloys and Compounds. 2005;399(1-2):245-50.
22. Verwey EJW, Haayman PW. Electronic conductivity and transition point of magnetite ("Fe3O4"). Physica. 1941;8(9):979-87.
23. Kolekar CB, Kamble PN, Kulkarni SG, Vaingankar AS. Effect of Gd3+ substitution on dielectric behaviour of copper-cadmium ferrites. Journal of Materials Science. 1995;30(22):5784-8.
24. Austin IG, Mott NF. Polarons in crystalline and non-crystalline materials. Advances in Physics. 1969;18(71):41-102.
25. Hogarth CA, Islam MH, Rahman ASMS. D.c. and a.c. electrical properties of vacuum evaporated thin SiO/GeO2 films. Journal of Materials Science. 1993;28(2):518-28.
26. Rahman MA, Rahman MA, Hossain AKMA. Effect of Cu2+ substitution on structural, magnetic and transport properties of Fe2.5Zn0.5−xCuxO4. Journal of Magnetism and Magnetic Materials. 2014;369:168-75.
27. Garai M, Sasmal N, Karmakar B. Effects of M2+ (M = Ca, Sr, and Ba) Addition on Crystallization and Microstructure of SiO2-MgO-Al2O3-B2O3-K2O-F Glass. Indian Journal of Materials Science. 2015;2015:1-8.
28. Koops CG. On the Dispersion of Resistivity and Dielectric Constant of Some Semiconductors at Audiofrequencies. Physical Review. 1951;83(1):121-4.
29. Yager WA. The Distribution of Relaxation Times in Typical Dielectrics. Physics. 1936;7(12):434-50.
30. Kharabe RG, Devan RS, Kanamadi CM, Chougule BK. Dielectric properties of mixed Li–Ni–Cd ferrites. Smart Materials and Structures. 2006;15(2):N36-N9.
31. Dutta S, Choudhary RNP, Sinha PK. Impedance spectroscopy studies on Ga-ion-modified PLZT ceramics. physica status solidi (a). 2005;202(6):1172-81.
32. M. Ramay S, A. Siddiqi S, Atiq S, S. Awan M, Riaz S. Structural, Magnetic, and Electrical Properties of Al3+ Substituted CuZn-ferrites. Chinese Journal of Chemical Physics. 2010;23(5):591-5.
33. Ramesh T, Shinde RS, Murthy SR. Synthesis and characterization of nanocrystalline Ni 0.94 Co 0.03 Mn 0.04 Cu 0.03 Fe 1.96−x Al x O 4 ferrites for microwave device applications. Journal of Magnetism and Magnetic Materials. 2013;345:276-81.
34. Hashim M, Alimuddin, Kumar S, Ali S, Koo BH, Chung H, et al. Structural, magnetic and electrical properties of Al3+ substituted Ni–Zn ferrite nanoparticles. Journal of Alloys and Compounds. 2012;511(1):107-14.
35. Mujasam Batoo K. Study of dielectric and impedance properties of Mn ferrites. Physica B: Condensed Matter. 2011;406(3):382-7.
36. Gul IH, Pervaiz E. Comparative study of NiFe2−xAlxO4 ferrite nanoparticles synthesized by chemical co-precipitation and sol–gel combustion techniques. Materials Research Bulletin. 2012;47(6):1353-61.
37. Ramesh B, Ramesh S, Kumar RV, Lakshmipathi Rao M. AC impedance studies on LiFe5−xMnxO8 ferrites. Journal of Alloys and Compounds. 2012;513:289-93.
38. Victor P, Bhattacharyya S, Krupanidhi SB. Dielectric relaxation in laser ablated polycrystalline ZrTiO[sub 4] thin films. Journal of Applied Physics. 2003;94(8):5135.
39. Ali MA, Uddin MM, Khan MNI, Chowdhury FUZ, Haque SM. Structural, morphological and electrical properties of Sn-substituted Ni-Zn ferrites synthesized by double sintering technique. J Magn Magn Mater. 2017;424:148-154.
40. Ali MA, Khan MNI, Chowdhury FUZ, Akhter S, Uddin MM. Structural Properties, Impedance Spectroscopy and Dielectric Spin Relaxation of Ni-Zn Ferrite Synthesized by Double Sintering Technique. Journal of Scientific Research. 2015;7(3):65-75.
41. Yakushiji K, Ernult F, Imamura H, Yamane K, Mitani S, Takanashi K, et al. Enhanced spin accumulation and novel magnetotransport in nanoparticles. Nature Materials. 2004;4(1):57-61.